JOURNAL OF MATERIALS SCIENCE 32 (1997) 741–747

Cyclic fatigue of long and short cracks in alumina

J. HEALY, A. J. BUSHBY, Y.-W. MAI
Centre for Advanced Materials Technology, Department of Mechanical and Mechatronic Engineering, University of Sydney, Sydney, New South Wales 2006, Australia

A. K. MUKHOPADHYAY
Electroceramics Division, Central Glass and Ceramic Research Laboratory, 196 Raja SC Mullick Road, Calcutta 700 032, India

The cyclic fatigue behaviour of long and microstructurally short cracks in a 10 μm grain-size alumina has been investigated. This material was found to be stress sensitive, a modest drop in applied stress resulting in a considerable lifetime enhancement. The growth of long cracks was studied using the circular compact tension geometry and was found to follow a Paris law behaviour. The crack path was entirely intergranular in this material with long fatigue crack growth governed by the degradation of crack-wake bridging. Short-crack growth was investigated using indented discs in a biaxial flexure geometry. Short cracks were observed to grow at lower values of applied ΔK than long cracks, increasing with crack length as bridging of the crack wake increased. The fatigue crack growth of AD90 alumina was also investigated by *in situ* testing within the specimen chamber of an SEM. The long-crack behaviour was found to be similar to the 10 μm grain-size alumina and other data reported in the literature. However, the crack path followed a mixture of transgranular and intergranular fracture and discontinuous in nature with frequent arrests. The crack-advancement mechanisms in these two alumina materials are different and affect the short-crack behaviour. However, in both cases the long-crack behaviour is dominated by crack-wake effects.

1. Introduction

The inherent brittleness of ceramics poses a major design problem from the perspective of structural reliability. Thus, given the fact that ceramics will contain flaws in spite of the best possible surface finish, an answer to the question of how long a component with a given flaw size is going to survive repeated loading, is desperately needed. Therefore, there has been a growing interest in the study of the cyclic fatigue and cyclic fatigue mechanisms in recent years. Lathabai *et al.* [1] conducted a comparison of static and cyclic lifetimes in water of alumina with a grain size of 23 μm. Evidence to support the view that slow crack growth dominated the fatigue response and that any other mechanical damage mechanism played an insignificant role in the degradation process, was presented. This was in keeping with earlier studies on alumina [2, 3]. A further study [4] on alumina with a coarsened grain size of 35 μm in water was conducted at stress levels below the static fatigue limit, which demonstrated true mechanical fatigue. Frictional degradation of bridging grains was identified as the cyclic fatigue process from *in situ* observations under vacuum. Ko [5, 6] investigated the effect of grain size on the fatigue strength of alumina under rotary bending. Two different grain sizes were investigated. An increase in fatigue strength was observed with a decrease in grain size from 28 μm to 10 μm. Guiu *et al.* [7] investigated both cyclic and static fatigue in a range of ceramic materials. Times to failure under cyclic loading were found to be shorter than under static loading. There have been numerous studies conducted on the long fatigue crack growth behaviour of a number of non-transformable ceramics [5–9]. A range of mechanisms has been proposed to account for the subcritical crack growth observed: degradation of bridging elements [7–11], possible microcracking and frictional sliding [8], wedging due to crack closure [10] and crack-path deflection or microcracking [9]. To date there has been relatively little work done on short-crack growth in these materials although a short-crack effect in magnesia partially-stabilized zirconia, akin to that in metals, has been reported by Steffen *et al.* [12] in which short cracks grow at stress intensities below the long cyclic fatigue crack threshold. A common method of initiating short cracks is to use a hardness indent. Hoside *et al.* [13] observed fatigue crack growth rates for both silicon nitride (Si_3N_4) and alumina (Al_2O_3) to follow a power law for differing applied stresses and indentation loads. However, the data were widespread. Horibe [14] and Horibe and Hirahara [15] also studied indentation

0022–2461

cracks, under four-point bending, in non-transformable ceramics. The data were examined in terms of crack length versus cycles. Neither studies compared short- and long-crack growth. This study reports preliminary results of fatigue crack growth in alumina in the two regimes of "physically short-" and long-crack growth.

2. Experimental procedure

2.1. Stress/life testing and short fatigue crack growth studies

Stress/life (S/N) testing and short fatigue crack growth studies were conducted on a nominally pure alumina, sintered from commercially available 99.99% pure powder (Morimura Bros. Inc., Tokyo, Japan). Sintering was carried out at a temperature of 1600 °C for 2 h. Density measurements by the water-immersion technique gave a value of 98% theoretical density. An average grain size of 10 μm was measured, using a polished and thermally etched sample in an image analyser. The hardness of this material, as measured by a Leitz Miniload Microhardness Tester, at a load of 500 g was 14.5 GPa. The fracture stress under monotonic loading was found to be 204 MPa.

Specimens in the form of 25 mm discs and 2 mm thickness were polished on the tensile surface to a finish of 1 μm. A 3.5 kg Vickers hardness indent was placed in the centre of the tensile face. The average surface crack length, from the centre of the indent to the surface crack tip was 64 μm.

All fatigue testing was carried out at a stress ratio of minimum to maximum stress of 0.1 at an average frequency of 10 Hz in ambient air using a servo-hydraulically controlled Instron 8501 fatigue machine. A biaxial test fixture was used which has the advantage over conventional four-point bending fixtures of not being susceptible to edge cracking. The stress was calculated from the following equation [16]

$$\sigma = \frac{3P(1+\nu)}{4\pi T^2}\left[1 + 2\ln\frac{r}{b} + \frac{(1-\nu)}{(1+\nu)} \times \left(1 - \frac{b^2}{2r^2}\right)\frac{r^2}{R^2}\right] \quad (1)$$

where P is the applied load, ν is Poisson's ratio, r is the radius of the support-ball ring, b is the radius of the loading flat, R is the specimen radius and T is the specimen thickness.

Short fatigue crack growth studies were conducted by periodically interrupting a number of S/N tests, removing the specimen and photographing the crack. The prints were then examined at a later stage and crack-growth increments determined.

The effective applied stress intensity factor at the crack tip is the sum of the stress intensity factor due to the applied load, K_a, and the residual stress intensity factor due to indentation, K_r, and is given by

$$K_{eff} = K_a + K_r \quad (2)$$

The remote applied stress intensity is given by

$$K_a = \psi\sigma_a(a + da)^{1/2} \quad (3)$$

where ψ is a geometry factor for a semi-circular crack [17], σ_a is the applied stress, a is the crack length and da the crack extension. This geometry was based on post-test analysis. In this study, cracks of several millimetres in length were occasionally observed. Clearly the crack front was not semi-circular; however, to limit errors, crack lengths longer than 1 mm were ignored for calculating stress intensity factors. This also limited the data to the "short-crack" regime.

The residual stress intensity factor arising from the indent is given by [18]

$$K_r = \xi\left(\frac{E}{H}\right)^{1/2}\frac{L}{(a + \mathrm{d}a)^{3/2}} \quad (4)$$

where ξ is a materially independent constant used for Vickers-produced radial cracks, E is the Young's modulus and L is the indentation load. Values of $\xi = 0.016$ [17], $E = 400$ GPa, $H = 14.5$ GPa and $P = 34.4$ N were used in this study.

2.2. Long fatigue crack studies

Long-crack fatigue tests were performed on the same 10 μm grain-size pure alumina in an attempt to compare directly long- and short-crack behaviour. The same disc-shaped specimens used for biaxial flexure experiments were tested in the circular compact tension geometry (CCT) (ASTM E-399). Specimens were precracked by placing a 20 kg Vickers indent orientated so that the radial cracks extended along the specimen axis. A slanting notch was then cut up to the indent site to leave one radial crack extending into the notch. Crack growth was monitored during tests through a travelling microscope using oblique transmitted illumination. Crack-length measurements were obtained, during periodic interruptions, by using an optical microscope in conjunction with an image analyser. Through-thickness crack growth was monitored over several millimetres while subjected to a tensile cyclic load at a stress ratio of 0.1 and a frequency of 10 Hz.

The stress intensity acting at the crack tip was calculated using Equation 2, where K_r is again given by Equation 4 (though it is recognized that notching may have reduced its magnitude by a considerable amount) and K_a in this case is given by

$$K_a = \left(\frac{P}{bw^{1/2}}\right)f(\alpha) \quad (5)$$

where P is the applied load, b the specimen thickness, w the specimen width, a is the crack length and $\alpha = a/w$. $f(\alpha)$ is given by

$$f(\alpha) = \frac{(2+\alpha)(0.76 + 4.8\alpha - 11.58\alpha^2 + 11.43\alpha^3 - 4.08\alpha^4)}{(1-\alpha)^{3/2}} \quad (6)$$

High-resolution optical microscopy techniques were developed using a Lietz DM RXE microscope to locate accurately the crack tip and monitor the crack-growth processes. At ×1000 magnification, and using

an intense offset illumination, it was possible to reveal detailed information regarding the nature of the crack-tip extension mechanism. Open cracks and fissures produced a strong contrast due to scattering of the light diffusing through the surface. Furthermore, visible features were not limited to the surface but could be resolved a few micrometres below the surface. By focusing through this range, open cracks could be readily identified.

2.3. Fatigue studies *in situ* on the SEM

Complementary long fatigue crack growth studies were carried out within the specimen chamber of the SEM using a commercially available alumina (AD90, Coor's Ceramic Co., USA) containing 10% impurities at the grain boundaries, the main impurities being silica, magnesia and calcia with small amounts of iron oxide, sodium oxide and potassium oxide. The manufacturer's data give the room-temperature tensile strength to be 221 MPa, the Young's modulus to be 276 GPa and the flexural strength to be 338 MPa. The grain size ranges from 2–10 μm, with an average size of 4 μm.

A beam of dimensions $6 \times 10 \times 50\,mm^3$ was polished to a finish of 1 μm. A thermal etch at 1500 °C under controlled heating and cooling rates served to dissipate the glassy phase and expose the surface crystal structure. A through-thickness precrack was then introduced into the beam, containing a single 50 kg Vickers indent, using a bridge compression method [19]. The precrack varied in length from $0.15 < \alpha < 0.4$, where α is the ratio of crack length to beam width. The beam was then sectioned into two lengthwise and ground to $2 \times 10 \times 50\,mm^3$. Long fatigue crack growth tests were carried out under vacuum using an *in situ* cycling device within the chamber of a Phillips 505 scanning electron microscope (SEM). Details of the technique are given elsewhere [20].

3. Results

3.1. Fatigue of 10 μm grain-size alumina

The lifetime (S/N) data for the indentation flaw specimens are shown in Fig. 1. The range of applied stress over which specimens failed varied from 97–132 MPa. The number of cycles to failure at similar applied stress levels could vary by as much as a factor of 6. However, at stress levels of 86, 94 and 97 MPa, specimens remained unbroken after a minimum of 2.25×10^6 cycles. The material shows a wide range of scatter and is stress sensitive. The value of the inverse slope, n, was found to be 22.7.

Typical variation of the surface crack length with the number of cycles is shown in Fig. 2. The crack growth from each side of the indent, measured from the centre of each indent is shown, together with the total surface crack length from tip to tip. There is good agreement between both sides indicating symmetrical loading.

Long- and short-crack data for the 10 μm pure alumina are compared in Fig. 3a as a function of the applied stress intensity range, ΔK_a. Data from CCT

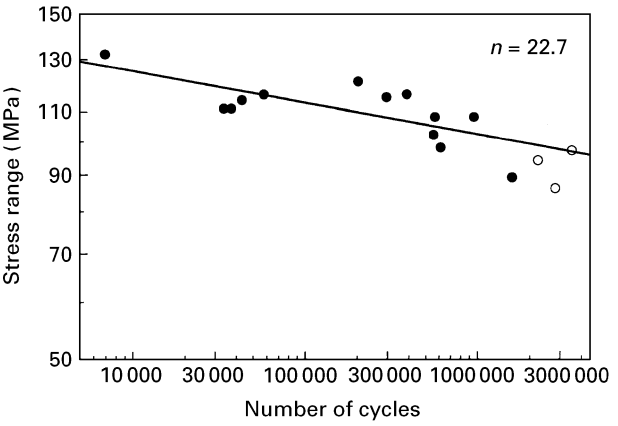

Figure 1 Cyclic fatigue graph of alumina, tested in air at a stress ratio of 0.1: (○) unbroken, (–●–) failed.

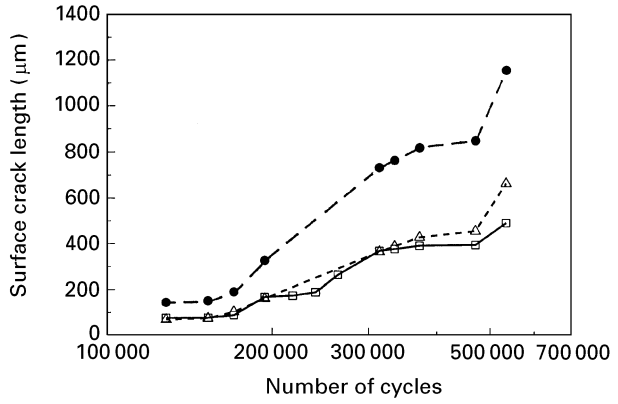

Figure 2 Variation of surface crack length with number of cycles elapsed, stress ratio $= 0.1$, $\sigma_{max} = 114$ MPa: (–□–) left side, (– –△– –) right side, (–●–) total length.

(long-crack) tests are seen to follow the usual Paris-law behaviour of the type

$$\frac{da}{dN} = C\Delta K^m \qquad (7)$$

with an exponent $m \approx 30$, which is a typical figure for this type of material. Data from biaxial flexure tests are also shown in Fig. 3a (short cracks), the numbers indicating crack length in sequence with the shortest having the lowest number. Short cracks from biaxial flexure tests greater than 250 μm also obey the Paris law for long cracks (Fig. 3a and b). Cracks with lengths less than 250 μm appear to grow at far lower ΔK_a values (1–2 MPa $m^{1/2}$), ΔK_a increasing systematically with increasing crack length up to 250 μm, whereafter the Paris law is obeyed. For these "short" cracks there is no obvious relation between crack growth rate, da/dN, and ΔK_a, in particular no "negative dependence" of da/dN on ΔK_a giving the V-shaped plots as reported by some authors [12, 13].

The crack path in this material was observed to be entirely intergranular, with the crack tip extending along grain boundaries. Large-scale crack-bridging ligaments were not observed in this material with contact between the crack faces, in general, limited to the scale of a grain size. Frictional contact between some grain facets could clearly be identified in the

crack wake and in some cases individual grains were dislodged, Fig. 4.

3.2. *In situ* testing of AD90

Data from long-crack tests in AD90 alumina are also included in Fig. 3b (*in situ*) and show very similar behaviour in spite of the difference in material and test conditions (vacuum on SEM). However, our *in situ* observations clearly showed that the long fatigue crack growth was discontinuous in nature with bursts of crack growth occurring over a few cycles after extended periods of cyclic loading. The growth rates presented are averaged over the entire cycling period and thus do not represent the true crack velocity.

The crack path observed during long-crack growth is presented in Fig. 5a, close to the crack tip, and at the crack tip Fig. 5b. These figures show the distribution of grain size in the AD90 material. Crack growth is predominantly transgranular and relatively large

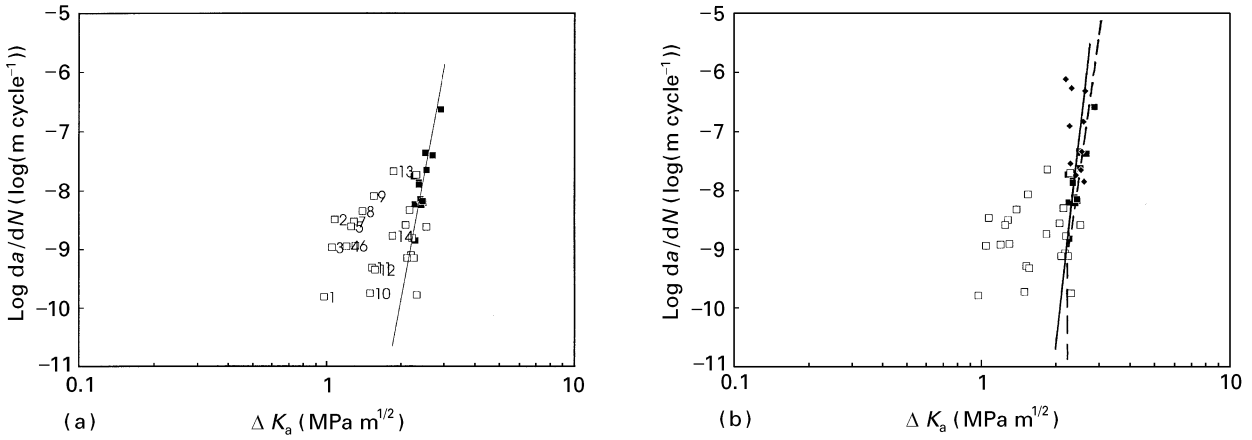

Figure 3 Crack velocity diagrams for aluminas tested. (a) 10 μm alumina in compact tension (■, long cracks) and biaxial flexure (□, short cracks). Numbers indicate increasing crack lengths. (b) 10 μm alumina in compact tension (■, long cracks) and biaxial flexure (□, short cracks) and for AD90 alumina (♦, *in situ*). (– – –) Data from Ogawa *et al.* [11] included for comparison.

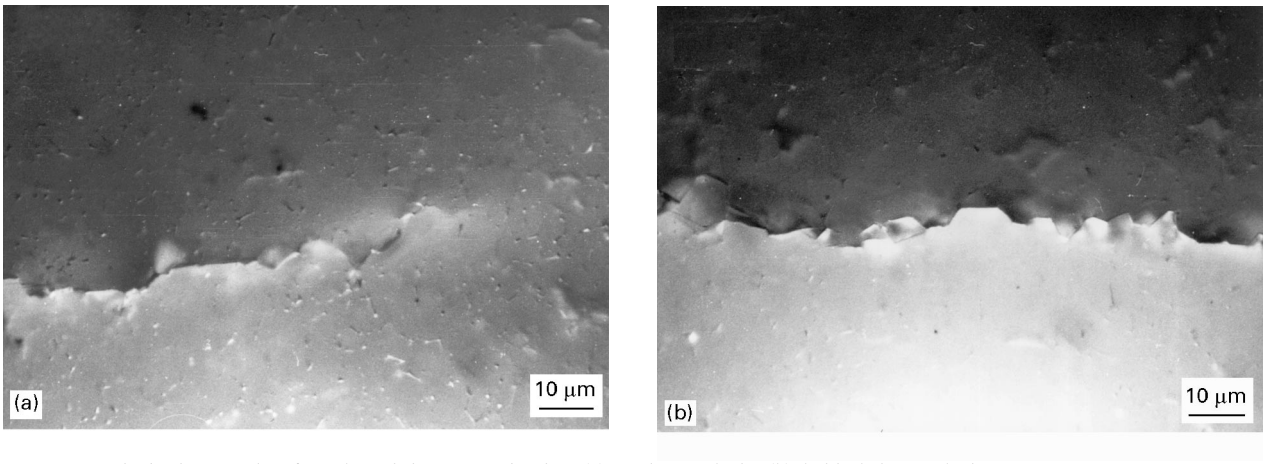

Figure 4 Optical micrographs of crack path in 10 μm alumina, (a) at the crack tip, (b) behind the crack tip.

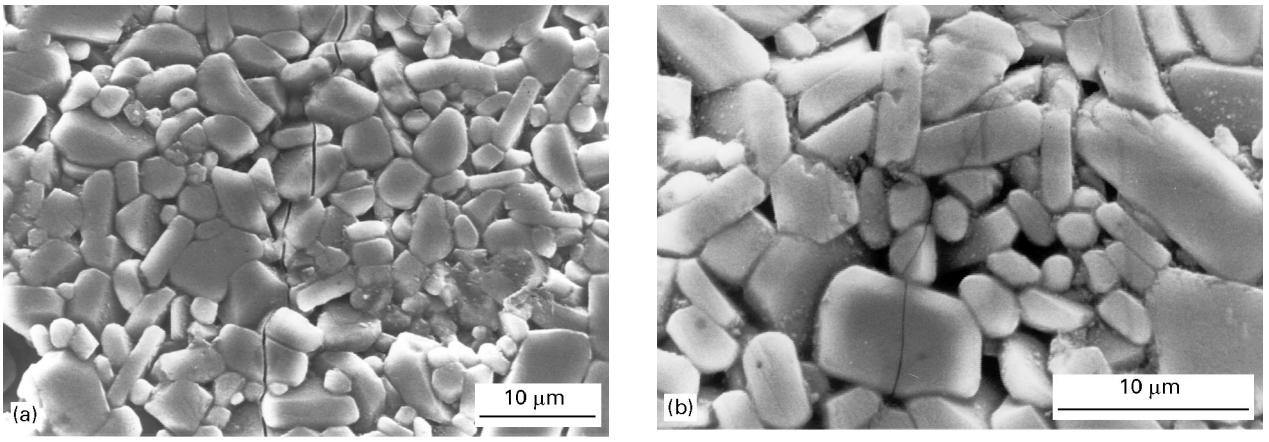

Figure 5 *In situ* observations of long fatigue crack in AD90, (a) behind the crack tip, (b) at the crack tip.

crack opening displacements (approximately 30 nm) can be seen, Fig. 5a. However, at the crack tip, the crack opening is unmeasurable and of the order of a few nanometres, Fig. 5b. After an increment of crack growth, the crack tip appeared to arrest mainly at grain boundaries, Fig. 6. However, the crack was also observed to arrest within a large grain (8 μm in length), Fig. 7a. A higher magnification micrograph, Fig. 7b, clearly illustrates this point as the crack is rendered visible by edge charging.

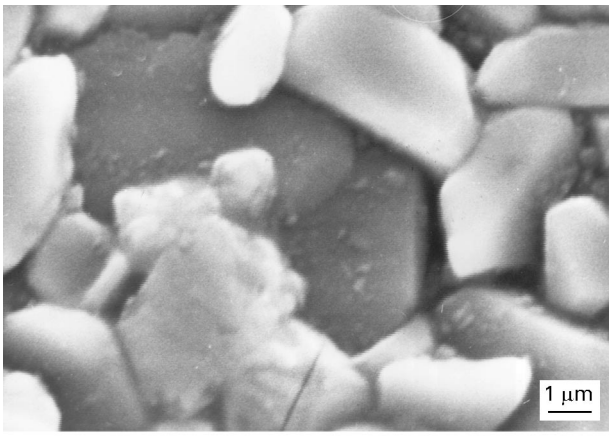

Figure 6 Crack tip arrested at a grain boundary in AD90.

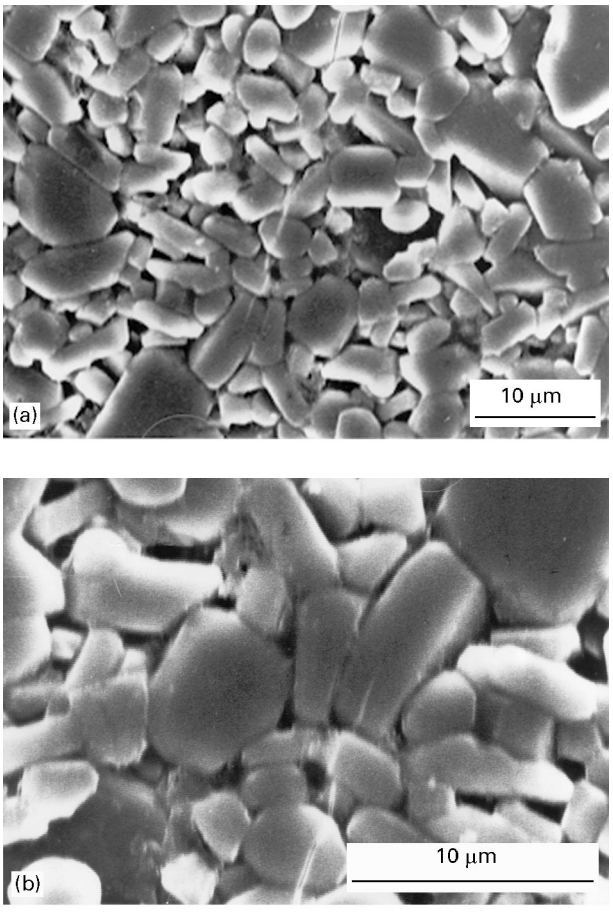

Figure 7 (a) Crack path in AD90 for a long crack, (b) Crack tip arrested in a large grain.

4. Discussion

The applied stress range over which the lifetime data shown in Fig. 1 were obtained (97–132 MPa) in air, is very similar to that reported by Lathabai *et al.* [4] (80–130 MPa) in water, for a coarser grain-sized material of 35 μm. In both cases the material was stress sensitive with a modest drop in strength corresponding to a marked change in the lifetime. This is in contrast with the results of Ko [6], who reported the S/N behaviour of two alumina ceramics, tested in ambient air. The smaller grained material (10 μm) could support higher cyclic loads when compared to the coarse-grained material (28 μm). However, this may be due to the inherently higher mechanical strength of fine-grained material because strength has an inverse dependence on grain size [20]. Direct comparison with the results of this study is not possible, as they were obtained by different test methodologies, rotating bend as opposed to biaxial flexure from samples containing a starter flaw (Vickers indent). Ko [6] observed a difference in macroscopic fracture features, with more branching evident in the finer grained material. However, no differences in fracture mechanisms were observed. The value of n reported in this study is within a range of values between 12.7 and 64 for a range of alumina ceramics, reported by Ko [6]. It is also similar to that reported by Guiu *et al.* [7] for both a 2 and 18 μm grain-sized alumina tested in ambient air, $n = 21$ and 23 respectively, as well as that reported by Ko [6] for a 10 μm grain-sized alumina of 19.3. S/N testing of alumina does not show a distinct knee, as is reported in metals or transformable ceramics [12]. While no failures were reported after 1.5×10^6 cycles in this study, with the longest test lasting 3.8×10^6 cycles, Ko [6] reported failure after tests in excess of 10^8 cycles for both aluminas tested. This raises a question concerning fatigue limits in this class of material, as in most cases a lifetime of 10^8 cycles would be considered as evidence of a fatigue limit.

Short fatigue crack growth is an area of interest in ceramics as their inherent brittleness, poor ductility and low toughness means that they will not tolerate long cracks in components which are in service. Catastrophic failure will thus be dominated by the behaviour of small flaws. This is an area which has not received much attention.

For the 10 μm alumina, crack growth proceeds entirely by intergranular fracture, presumably assisted by tensile residual stresses at some grain boundaries due to thermal expansion anisotropy. This tortuous crack path introduces bridging sites in the crack wake as it progresses. This gives rise to an additional term, K_b, due to wake bridging in Equation 2. In reality as the crack wake bridges are developed, an R-curve is obtained. It appears that under these testing conditions, the maximum length of the fully developed bridging zone is about 250 μm. For fatigue cracks longer than this length, the crack growth depends on the degradation of crack-wake bridges due to cyclic loading. A discussion on this topic has been given by Hu and Mai [21]. It is shown here that the short cracks do not follow the long-crack Paris law and crack growth is not governed solely by the applied

stress intensity range. However, short cracks in the biaxial flexure test are strongly influenced by the residual stress field associated with the indentation which imparts a large static component, K_r, to the total K_{eff}. For short cracks there may be some doubt as to the accuracy of Equation 4 for K_r. Furthermore, it was not always possible to determine crack shape. The assumption of a half-penny shaped crack for the calculation of a stress intensity factor, as also assumed in other studies [1, 4, 15], may be open to question and partly responsible for the degree of scatter in the short-crack data. However, the graph of surface crack length, Fig. 2, would appear to indicate that this is a valid method of obtaining short-crack data. Additionally, because bridging sites in short cracks, on the scale of the microstructure, would be less bridged than long cracks, the bridging effect due to K_b is much less pronounced. These differences in K_b lead to different da/dN results as reflected in the log-log plot of da/dN versus ΔK_a in Fig. 3a.

AD90 shows a mixture of intergranular and transgranular crack growth occurring in short bursts with crack arrest at grain boundaries (Fig. 6) and at times within a single grain (Fig. 7). Ogawa *et al.* [11] also noted discontinuous crack growth in their studies using a conducting surface film technique to record the crack growth. This implies that the crack-tip extension mechanism is different to the pure alumina, being both transgranular and intergranular. However, in both materials the long-crack behaviour is dominated by crack-wake effects and so the fatigue behaviour is similar, both following the Paris law with a similar exponent. This implies that for short or microstructurally small cracks, the fatigue crack growth behaviour is highly dependent on the local microstructure and mechanism of crack extension. Intermediate behaviour consists of an increasing bridging effect until saturation is reached, in the case of 10 μm alumina, at a crack length of 250 μm.

The *in situ* cyclic fatigue results of this study are in good agreement with the long-crack studies of Ogawa *et al.* [11] carried out on the same material in air, the slope being reported as 29.4 (Fig. 3b). The *in situ* studies were carried out under vacuum; crack growth is therefore the result of true mechanical fatigue, whereas the studies of Ogawa *et al.* [11] were conducted in air and combine the influence of both static (or environmentally assisted) fatigue as well as cyclic (or mechanical) fatigue. Thus it would appear that in this material (AD90), the cyclic contribution to fatigue crack growth is predominant. The crack-growth data are limited to two decades of crack growth rates. This is a reflection of the limited regime of stable crack growth (threshold at 2.2 MPa $m^{1/2}$ and K_{Ic} at 3.3 MPa $m^{1/2}$ [11]).

Studies on natural flaws in Mg–PSZ [12] revealed a short-crack effect when compared to long fatigue cracks in terms of the crack-tip stress intensity. The data were normalized by taking into account crack-tip shielding due to phase transformation. There are no previously published studies which compared short and long fatigue crack growth in the same alumina materials.

The observations of crack bridging for long fatigue cracks, Figs 4 and 5, are consistent with the results of other workers [4, 7, 21–24] on a range of alumina ceramics under both monotonic and cyclic loading. Based on electron microscopic evidence of bridging grains in the crack wake, it may be reasonable to assume that frictional degradation of these grain bridges or ligaments during cyclic loading was the main mechanism of fatigue crack growth, as suggested by other workers [4]. The *in situ* SEM observations of long-crack growth point to intergranular crack growth being important in fatigue crack growth resistance. From the crack opening displacements it is clear that crack closure behind the crack tip is not playing any significant role in the mechanical fatigue process. Although no fretting or bridging grains were observed as previously reported [4], there was a degree of tortuosity in the crack path that suggests that a frictional component at the grain boundaries is the main mechanism of resistance in this material. The local deflection due to intergranular crack growth is most clearly illustrated in Fig. 5a. The large amount of transgranular crack growth is responsible for the low fracture toughness of this material. Recent work by Guiu *et al.* [10], inferred from the analysis of compliance measurements of long cracks, has suggested that the elastic component of bridging ligaments is greater than the frictional component and that shielding increases with increased grain size. However, the behaviour of short cracks is likely to be more strongly influenced by microstructural and crack-path factors.

5. Conclusion

The cyclic fatigue response of an indented 10 μm grain-sized alumina has been investigated under biaxial loading and characterized by evaluation of the stress/life (S/N) behaviour and short fatigue crack growth rates. From S/N data, a similar exponent to that reported by other workers in aluminas of varying grain sizes was obtained. Long fatigue crack growth rates were also evaluated for this material using the circular compact tension geometry. The long fatigue crack growth response of a commercially available alumina (AD90) under vacuum was also studied. From optical and electron microscopic examination, it appears that frictional degradation of bridging grains in the crack wake is the main mechanism of cyclic crack growth once the crack-wake bridging zone is fully developed. For short cracks, where the bridging effect is reduced, the crack-advance mechanism is highly dependent on the microstructure and does not depend solely on the cyclic applied stress intensity range, ΔK_a.

Acknowledgements

The cooperation, support and provision of facilities by the Department of Civil Engineering and the Electron Microscope Unit at the University of Sydney are gratefully acknowledged as is the continuing financial support of the Australian Research Council for this project.

References

1. S. LATHABAI, Y.-W. MAI and B. R. LAWN, *J. Am. Ceram. Soc.* **72** (1989) 1760.
2. A. G. EVAN and E. R. FULLER, *Metall. Trans.* **5A** (1974) 27.
3. D. A. KROHN and D. P. H. HASSELMAN, *J. Am. Ceram. Soc.* **55** (1972) 208.
4. S. LATHABAI, J. RODEL and B. R. LAWN, *ibid.* **74** (1991) 1340.
5. H. N. KO, *J. Mater. Sci. Lett.* **5** (1986) 464.
6. *Idem*, *ibid.* **8** (1989) 1438.
7. F. GUIU, M. J. REECE and D. A. J. VAUGHAN, *J. Mater. Sci.* **26** (1991) 3275.
8. L. EWART and S. SURESH, *ibid.* **22** (1987) 1173.
9. M. OKAZAKI, A. J. McEVILY and T. TANAKA, *Metall. Trans.* **22A** (1991) 1425.
10. F. GUIU, M. LI and M. J. REECE, *J. Am. Ceram. Soc.* **75** (1992) 2976.
11. T. OGAWA, T. OCHI and K. TOKAJI, *Fat. Fract. Eng. Mater. Struct.* **16** (1993) 837.
12. A. A. STEFFEN, R. H. DAUSKARDT and R. O. RITCHIE, *J. Am. Ceram. Soc.* **74** (1991) 1259.
13. T. HOSIDE, T. OHARA and T. YAMADA, *Int. J. Fract.* **37** (1988) 47.
14. S. HORIBE, *J. Mat. Sci. Lett.* **7** (1988) 725.
15. S. HORIBE, and N. HIRAHARA, *Acta. Metall. Mater.* **39** (1991) 1309.
16. R. THIRUVENGADSWAMY and R. O. SCATTERGOOD, *Scripta Metall. Mater.* **25** (1991) 2529.
17. R. F. CLARKE and D. R. COOK, *Acta Metall.* **36** (1988) 555.
18. C. R. ANNTIS, P. CHANTIKUL, B. R. LAWN and D. B. MARSHALL, *J. Am. Ceram. Soc.* **25** (1981) 533.
19. Japanese Industrial Standard (JIS) R 1607, published by the Japanese Standards Association, Japan (1990).
20. P. CHANTIKUL, S. J. BENNISON and B. R. LAWN, *J. Am. Ceram. Soc.* **73** (1990) 2419.
21. X.-Z. HU and Y.-W. MAI, *ibid.* **75** (1992) 848.
22. G. VENKINIS, M. F. ASHBY and P. W. R. BEAUMONT, *Acta Metall. Mater.* **38** (1990) 1151.
23. P. L. SWANSON, C. J. FAIRBANKS, B. R. LAWN, Y.-W. MAI and B. J. HOCKEY, *J. Am. Ceram. Soc.* **70** (1987) 279.
24. J. RODEL, J. F. KELLY and B. R. LAWN, *ibid.* **73** (1990) 3313.

Received 7 June
and accepted 20 November 1995